PETROPHYSICS, VOL. 45, NO. 2 (MARCH-ARPIL 2004); P. 167–178; 17 FIGURES

Fast 3D Imaging from a Single Borehole Using Tensor Induction Logging Data

Michael S. Zhdanov[1], Efthimios Tartaras[2], and Alexander Gribenko[1]

ABSTRACT

There is growing interest in the development of new borehole electromagnetic (EM) induction methods capable of characterizing the conductivity distribution in the space surrounding the borehole. The main goal of this paper is to develop a method of three-dimensional (3-D) imaging from a single borehole using a tri-axial (tensor) induction instrument. The tensor instrument has a directional sensitivity, which allows finding the correct location of the 3-D resistive and conductive targets from single-hole data. Our method is based on the novel localized quasi-linear (LQL) approximation. The LQL approximation is specially designed for modeling the electromagnetic field generated with a moving transmitter, which is the case for borehole induction logging. The traditional approach to electromagnetic modeling and inversion requires multiple solutions for different transmitter positions. The LQL approximation makes it possible to run the forward and inverse problem at once for all the transmitters, which makes the inversion of the well-logging data much more efficient. Our study demonstrates that this method can be effectively used for 3-D imaging from a single borehole.

INTRODUCTION

The electromagnetic (EM) induction method is one of the most powerful techniques for formation conductivity (or resistivity) evaluation. The practical application of this method in well logging was inspired by the pioneering work of Doll (1949). For more than half a century the basic interpretation model of induction logging was a cylindrically symmetrical model of the rocks surrounding the borehole. The symmetrical structure of the model was dictated by the fact that the standard induction instrument, with the transmitter and receiver oriented along the borehole axis, had axially symmetric sensitivity. However, the real geological structures in the vicinity of the borehole are much more complicated. Today, there is growing interest in developing new borehole EM induction methods capable of characterizing the conductivity distribution in the space surrounding the borehole. It was demonstrated in the papers by Portniaguine and Zhdanov (1999a) and Alumbaugh and Wilt (2001) that a new three-component induction logging instrument can be used for three-dimensional (3D) imaging about a single borehole. This instrument has three mutually perpendicular magnetic induction receiver coils and three magnetic induction transmitter coils. It was shown by Sato et al. (1996), Cheryauka et al. (2001), and in the papers cited above, that this instrument has directional sensitivity to off-borehole axis geoelectrical structures. This instrument detects three components of the magnetic field due to each of three transmitters, which form an induction tensor. The tri-axial induction instrument was originally introduced to resolve formation anisotropy (Moran and Gianzero, 1978; Moran, 1981; Kriegshauser et al. 2000, 2001; Zhdanov et al., 2001a,b). However, another important area for application of this tool is to study the 3D distribution of the conductivity in the media surrounding the

Manuscript received by the Editor September 20, 2002, revised manuscript received November 6, 2003.
[1]University of Utah, Department of Geology and Geophysics, Salt Lake City, UT 84112, USA
[2]Currently with Schlumberger Riboud Product Centre, 92142 Clamart, France

borehole, which can provide unique information, for example, about asymmetry of the invaded zone, the location of the petroleum reservoir or the oil-water contact in the case of a deviated or horizontal well.

Thus, the main goal of this paper is to develop a method of 3D imaging from a single borehole using a tri-axial (tensor) induction instrument. Our method is based on the novel localized quasi-linear (LQL) approximation, introduced by Zhdanov and Tartaras (2002) for airborne EM data interpretation. This approximation was specially designed for modeling the EM field generated with a moving transmitter, which is the case for borehole induction logging. The traditional approach to EM modeling requires multiple solutions for different transmitter positions, which is an extremely time consuming technique. The LQL approximation makes it possible to run the forward and inverse problem at once for all the transmitters, which makes the inversion of the well-logging data much more efficient.

Finally, we believe that this newly developed technique for 3D imaging from a single borehole opens a new possibility for 3D reservoir characterization, which can help significantly in the future construction of more realistic models of petroleum reservoirs using geophysical well-logging data.

LQL APPROXIMATION IN THE BOREHOLE IMAGING

The main difficulties in modeling and interpretation of induction logging data in 3D inhomogeneous formations are related to the fact that for any new observation point, one has to solve the forward problem anew for the corresponding position of the moving transmitter. In this situation, even forward modeling of the well logging data over inhomogeneous structures requires an enormous number of computations. The inversion of the logging data becomes even more time consuming because it requires repeated forward modeling with the updated model parameters. Practically speaking, full 3D inversion of the induction borehole data based on the rigorous forward modeling method may require several days of continuous computations on modern computers even in the case of simple interpretation models. It is obvious that this kind of interpretation is unacceptable for analysis of well logging data in industry.

In order to overcome this difficulty we apply for the inversion of the induction well logging data a new mathematical method developed recently by the Consortium for Electromagnetic Modeling and Inversion (CEMI). This method is based on the novel approximate, but accurate, method of forward modeling, the so-called localized quasi-linear (LQL) approximation (Zhdanov and Tartaras, 2002; Zhdanov, 2002). The LQL approximation is a powerful instrument for fast 3D modeling and inversion of multi-source EM geophysical data. It has been successfully applied to the modeling and inversion of airborne EM data collected for mineral exploration (Tartaras et al., 2001). We will demonstrate in this paper that a similar approach can be used in borehole geophysics where fast 3D imaging is required.

Consider a 3D geoelectrical model of the rock formations with background conductivity σ_b and local inhomogeneity D with arbitrary spatial variations of conductivity $\sigma = \sigma_b + \Delta\sigma$. The background conductivity represents a layered formation, which may consist of an arbitrary number of homogeneous layers with different conductivities and thicknesses. In principle, the background model can be formed by anisotropic layers as well, however, for the sake of simplicity, in this paper we restrict our study to isotropic formations only. Note that the background model may also include the effect of the borehole. We assume that the background distribution of the conductivity is known, based, for example, on the results of conventional induction well logging. The anomalous conductivity is the target of the inversion. It characterizes any variation of the true conductivity from a given background model,

$$\Delta\sigma = \sigma - \sigma_b$$

and can be positive (for a conductive zone) or negative (for a resistive zone, for example).

The electromagnetic fields in this model can be presented as a sum of background and anomalous fields

$$\mathbf{E} = \mathbf{E}^b + \mathbf{E}^a, \quad \mathbf{H} = \mathbf{H}^b + \mathbf{H}^b, \tag{1}$$

where the background field is the field generated by the given transmitter in the model with the background distribution of conductivity σ_b, and the anomalous field is produced by the anomalous conductivity distribution Δ_b.

A tri-axial electromagnetic induction instrument detects three components of the total magnetic field due to each of three transmitters. In the framework of the integral equation (IE) numerical modeling method, the anomalous magnetic field, $\mathbf{H}^a$, due to a 3D anomalous domain D, with anomalous conductivity, $\Delta\sigma$, located outside a borehole in a layered background, is given as an integral of the product of the anomalous conductivity and the total electric field over the anomalous domain D (Zhdanov, 2002)

$$\mathbf{H}^a(\mathbf{r}_j) = \iiint_D \hat{G}_H(\mathbf{r}_j|\mathbf{r}) \cdot \Delta\sigma[\mathbf{E}^b(\mathbf{r}) + \mathbf{E}^a(\mathbf{r})]dv = \mathbf{G}_H[\Delta\sigma(\mathbf{E}^b + \mathbf{E}^a)], \tag{2}$$

where $\hat{\mathbf{G}}_H(\mathbf{r}_j|\mathbf{r})$ is the magnetic Green's tensor defined for

an unbounded conductive medium with the background conductivity σ_b, and $\mathbf{G}_H$ is the magnetic Green's linear operator.

Note that a similar integral representation can be written for the anomalous electric field

$$\mathbf{E}^a(\mathbf{r}_j) = \iiint_D \hat{G}_E(\mathbf{r}_j|\mathbf{r}) \cdot \Delta\sigma[\mathbf{E}^b(\mathbf{r}) + \mathbf{E}^a(\mathbf{r})]dv = \mathbf{G}_E[\Delta\sigma(\mathbf{E}^b + \mathbf{E}^a)], \quad (3)$$

where $\hat{\mathbf{G}}_H(\mathbf{r}_j|\mathbf{r})$ is the electric Green's tensor and $\mathbf{G}_E$ is the electric Green's linear operator (Zhdanov, 1988).

Our goal is to find the anomalous conductivity from the given measurements of the anomalous magnetic field by the moving tri-axial induction instrument. Equation (2) describes a nonlinear inverse problem, because the anomalous electric field is also a function of the anomalous conductivity $\Delta\sigma$. In the framework of the LQL approximation, we assume that the anomalous electric field inside the anomalous domain is linearly proportional to the background electric field through an electrical reflectivity tensor $\hat{\lambda}(\mathbf{r})$,

$$\mathbf{E}^a = \hat{\lambda}(\mathbf{r}) \cdot \mathbf{E}^b(\mathbf{r}), \quad (4)$$

which is assumed to be source independent. The validity of this assumption was demonstrated by Zhdanov and Tartaras (2002). Substituting expression (4) back into (2), we find

$$\mathbf{H}^a(\mathbf{r}_j) = \mathbf{G}_H\left\lfloor \Delta\sigma(\mathbf{r})\left(\hat{\mathbf{I}} + \hat{\lambda}(\mathbf{r})\right) \cdot \mathbf{E}^b(\mathbf{r}) \right\rfloor = \mathbf{G}_H[\hat{\mathbf{m}}(\mathbf{r}) \cdot \mathbf{E}^b(\mathbf{r})], \quad (5)$$

where $\hat{\mathbf{I}}$ is the identity tensor, and

$$\hat{\mathbf{m}}(\mathbf{r}) = \Delta\sigma(\mathbf{r})\left(\hat{\mathbf{I}} + \hat{\lambda}(\mathbf{r})\right), \quad (6)$$

is a material property tensor, which is also source independent.

We can consider now a new inverse problem (5) with respect to tensor $\hat{\mathbf{m}}$, which is a linear problem. Note that this linear problem is formulated for all possible transmitter and receiver positions simultaneously, meaning that we can process all observations obtained with the tri-axial instrument moving along the borehole at once! Thus, by using the LQL approximation we arrive at one linear inverse problem for the entire observation array.

After determining tensor $\hat{\mathbf{m}}$, we can find electrical reflectivity tensor $\hat{\lambda}$. The solution of this problem is based on the following consideration. Substituting formula (4) into (3), we obtain the quasi-linear (QL) approximation $\mathbf{E}^a_{QL}(\mathbf{r}_j)$ for the anomalous electric field

$$\mathbf{E}^a_{QL}(\mathbf{r}_j) = \mathbf{G}_E\left\lfloor \Delta\sigma(\mathbf{r})\left(\hat{\mathbf{I}} + \hat{\lambda}(\mathbf{r})\right) \cdot \mathbf{E}^b(\mathbf{r}) \right\rfloor = \mathbf{G}_E[\hat{\mathbf{m}}(\mathbf{r}) \cdot \mathbf{E}^b(\mathbf{r})]. \quad (7)$$

Following Habashy et al. (1993), and Torres-Verdin and Habashy (1994), we can take into account that the Green's tensor $\hat{\mathbf{G}}_E(\mathbf{r}_j|\mathbf{r})$ exhibits either singularity or a peak at the point where $\mathbf{r}_j = \mathbf{r}$. Therefore, one can expect that the dominant contribution to the integral $\hat{\mathbf{G}}_E\lfloor \hat{\mathbf{m}} \cdot \mathbf{E}^b \rfloor$ in equation (7) is from some vicinity of the point $\mathbf{r}_j = \mathbf{r}$. Assuming also that the background field $\mathbf{E}^b$ is slowly varying within domain D, one can rewrite equation (7)

$$\mathbf{E}^a_{QL}(\mathbf{r}_j) \approx \mathbf{G}_E[\hat{\mathbf{m}}(\mathbf{r})] \cdot \mathbf{E}^b(\mathbf{r}_j), \quad (8)$$

where the tensor Green's operator $\mathbf{G}_E[\hat{\mathbf{m}}(\mathbf{r})]$ is given by the formula

$$\mathbf{G}_E[\hat{\mathbf{m}}(\mathbf{r})] = \iiint_D \hat{\mathbf{G}}_E(\mathbf{r}_j|\mathbf{r}) \cdot \hat{\mathbf{m}}(\mathbf{r})dv. \quad (9)$$

Comparing equations (4) and (8), we find that

$$\mathbf{E}^a_{QL}(\mathbf{r}_j) \approx \hat{\lambda}(\mathbf{r}_j) \cdot \mathbf{E}^b(\mathbf{r}_j) \approx \mathbf{G}_E[\hat{\mathbf{m}}(\mathbf{r})] \cdot \mathbf{E}^b(\mathbf{r}_j).$$

Therefore, the electrical reflectivity tensor can be determined from the solution of the minimization problem,

$$\left\| \hat{\lambda}(\mathbf{r}_j) \cdot \mathbf{E}^b(\mathbf{r}_j) - \mathbf{G}_E[\hat{\mathbf{m}}(\mathbf{r})] \cdot \mathbf{E}^b(\mathbf{r}_j) \right\|_{L_2(D)} = \min. \quad (10)$$

Taking into account that

$$\left\| \hat{\lambda}(\mathbf{r}_j) \cdot \mathbf{E}^b(\mathbf{r}_j) - \mathbf{G}_E[\hat{\mathbf{m}}(\mathbf{r})] \cdot \mathbf{E}^b(\mathbf{r}_j) \right\|_{L_2(D)} \le \left\| \hat{\lambda}(\mathbf{r}_j) - \mathbf{G}_E[\hat{\mathbf{m}}(\mathbf{r})] \right\|_{L_2(D)} \left\| \mathbf{E}^b(\mathbf{r}_j) \right\|_{L_2(D)},$$

we can substitute the minimization problem (10) by another problem

$$\left\| \hat{\lambda}(\mathbf{r}_j) - \mathbf{G}_E[\hat{\mathbf{m}}(\mathbf{r}_j)] \right\|_{L_2(D)} = \min. \quad (11)$$

The solution of equation (11) gives us *a localized electrical reflectivity tensor*, which is obviously source independent.

Finally, we find $\Delta\sigma$ from equation (6). Note that equation (6) should hold for any frequency, because the electrical reflectivity and the material property tensors are functions of frequency as well: $\hat{\lambda} = \hat{\lambda}(\mathbf{r}, \omega)$, $\hat{\mathbf{m}} = \hat{\mathbf{m}}(\mathbf{r}, \omega)$. In reality, of course, it holds only approximately. Therefore, the con-

ductivity $\Delta\sigma(\mathbf{r})$ can be found by using the least square method of solving equation (6)

$$\left\|\hat{\mathbf{m}}(\mathbf{r},\omega)-\Delta\sigma(r)(1+\hat{\lambda}(\mathbf{r},\omega))\right\|_{L_2(\omega)}=\min. \qquad (12)$$

This inversion scheme can be used for any multisource technique, since $\hat{\lambda}$ and $\hat{\mathbf{m}}$ are source independent. This reduces the original nonlinear inverse problem (2) to three linear inverse problems: the first one, equation (5) for the tensor $\hat{\mathbf{m}}$, another one, equation (11) for the parameter $\hat{\lambda}$, and the third one, equation (12) for the anomalous conductivity $\Delta\sigma$.

The computational aspects of the solution of the linear inverse problem (5), determination of the reflectivity tensor $\hat{\lambda}$, and the anomalous conductivity $\Delta\sigma$, are analyzed in Zhdanov and Tartaras (2002). We refer interested readers to this paper for numerical details.

FOCUSING REGULARIZED INVERSION TECHNIQUE

Note that inverse problem (5) is an ill-posed problem. The solution of this problem requires application of the corresponding regularization methods (Tikhonov and Arsenin, 1977). The traditional way to implement regularization in the solution of the inverse problem is based on a consideration of the class of inverse models with a smooth distribution of the model parameters. Within the framework of classical Tikhonov regularization, one can select a smooth solution by introducing the corresponding minimum norm, or "smoothing" stabilizing functionals. This approach is widely used in geophysics and has proven to be a powerful method for the stable inversion of geophysical data.

The traditional inversion algorithms providing smooth solutions for geoelectrical structures have difficulties, however, in describing the sharp geoelectrical boundaries between different geological formations. This problem arises, for example, in inversion for the local resistive or conductive target with sharp boundaries between the resistor/conductor and the host rocks, which is a typical model in well logging. For example, these kinds of models are used in oil-water contact monitoring and other reservoir study applications. In these situations, it can be useful to search for a stable solution within the class of inverse models with sharp geoelectrical boundaries. The solution of this problem is based on introducing a special type of stabilizing functional, the so-called minimum support or minimum gradient support functionals (Portniaguine and Zhdanov, 1999b; Zhdanov, 2002). We call this technique "focusing regularized inversion," to distinguish it from the traditional smooth regularized inversion. Our inversion code uses the re-weighted conjugate gradient method (Zhdanov, 2002), which can incorporate both the smooth regularized inversion, generating a smooth image of the inverted resistivity, and a focusing regularized inversion, producing a sharp focused image of the geoelectrical target. Some examples of smooth and focused inversion will be shown below.

The basic principles of Tikhonov regularization with the focusing stabilizers and the mathematical techniques for solving this problem are described in details in the monograph by Zhdanov (2002). We refer the interested reader to this publication to learn more about this new development in inversion theory.

NUMERICAL MODELING OF 3D IMAGING ABOUT A SINGLE BOREHOLE

In this section we illustrate the developed method of 3D imaging from a single borehole using numerical modeling. Note that in this early stage of the development of a new 3D imaging technology, we evaluate our method on a set of simple models of local inhomogeneities located in the vicinity of the borehole to demonstrate that the developed method is capable of solving this problem. In future, we plan to investigate more realistic models of rock formations. The major point is that with the tri-axial induction tool the "well logging world" should no longer be treated as one-dimensional (1D), but can adequately represent the real 3D geology.

We consider two types of logging instruments. The first consists of one transmitter oriented along a borehole axis and two triples of mutually orthogonal receivers located at the distances 0.33 m and 1 m from the transmitter respectively (Figure 1). The second instrument comprises three mutually orthogonal transmitter coils located at one point and similar receiver coils located at another point (Figure 8). We have chosen these basic instrument designs, because practical tools with similar designs are available now for well logging applications. At the same time, this modeling study will demonstrate that the developed imaging method is not restricted to any one specific induction logging instrument design and can be used, in principal, with arbitrary transmitter-receiver configurations.

Figure 2 shows Model 1 of a resistive layer located on one side of the borehole. The background conductivity is of 0.25 S/m and the anomalous conductivity is of -0.24 S/m. The instrument, shown in Figure 1, is moving in the vertical direction with observation points located every 1 m. The operating frequencies used for simulating the synthetic well logging data are 1, 10, and 100 KHz. In Figure 2, the transmitter locations are highlighted by the stars. Whilst this model may not be seen as a realistic petrophysical model, the main goal of this numerical experiment is to demon-

strate that the LQL inversion can correctly determine the asymmetrical location of the resistive formation on one side of the borehole. The synthetic magnetic data for this model were computed using the integral equation forward modeling code INTEM3D developed by CEMI consortium (Hursan and Zhdanov, 2002). The data were contaminated by 2% random noise. The solid lines in Figure 3 present the vertical profiles of the real parts of the x, y, and z magnetic components computed in the receivers. Figure 4 shows the imaginary parts of the same components (solid lines).

For the inversion we chose a volume of 5 x 5 x 10 m symmetrical around the borehole axis, from -2.5 to 2.5 m in the x direction, from -2.5 to 2.5 m in the y direction, and from 0 to 10 m in the vertical direction. This volume is subdivided into 10 cells in each direction for a total of 1000 cells. The size of one cell is 0.5 x 0.5 x 1 m. Figure 5 presents the

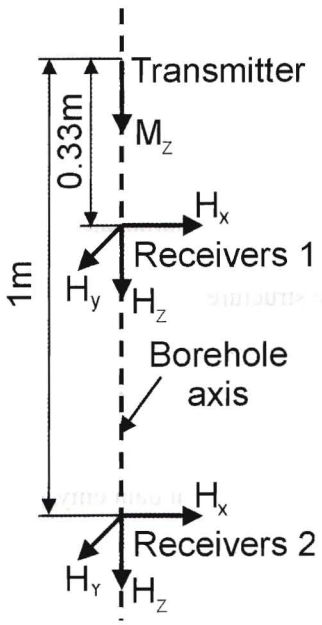

FIG. 1 Tri-axial induction instrument with one transmitter oriented along a borehole axis and two triples of mutually orthogonal receivers located at the distances 0.33 m and 1 m from the transmitter respectively.

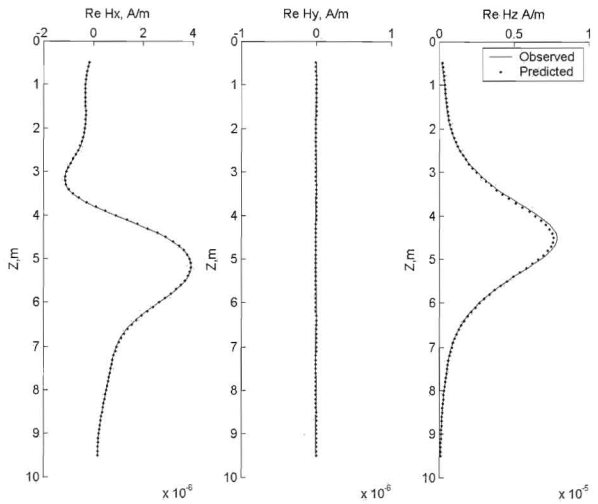

FIG. 3 The vertical profiles of the real parts of the x, y, and z magnetic components recorded by the three-component receivers for Model 1.

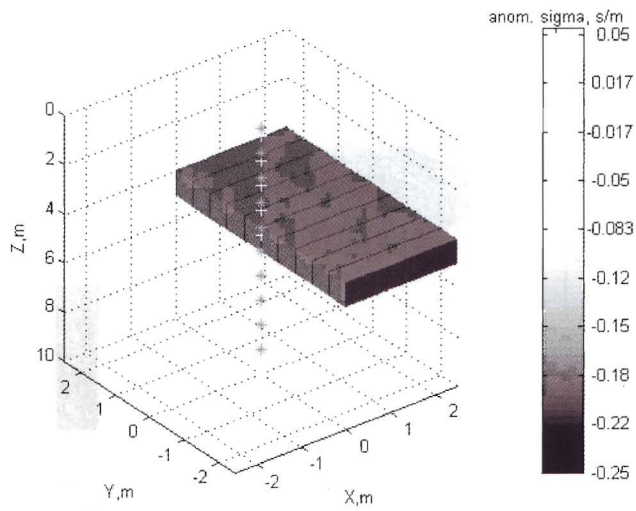

FIG. 2 Model 1 of a resistive layer located on one side of the borehole. The transmitter locations are shown by the stars.

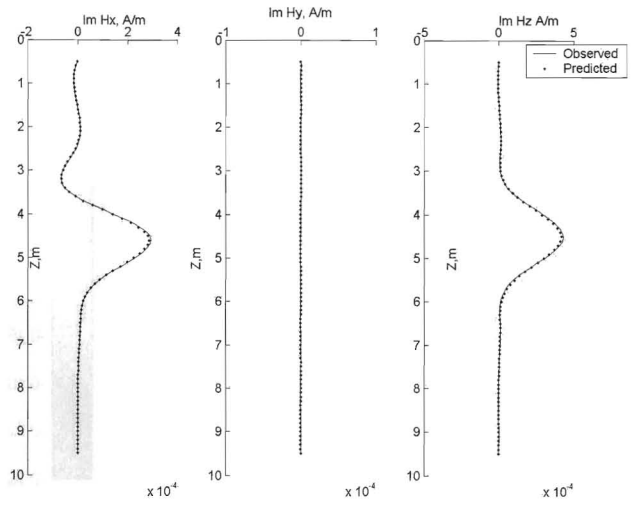

FIG. 4 The vertical profiles of the imaginary parts of the x, y, and z magnetic components recorded by the three-component receivers for Model 1.

smooth inversion result for Model 1. This figure shows the correct depth of the resistive layer. However, the resistive structure is seen on both sides of the reservoir, which does not agree with the true model. At the same time, the image is diffused and unclear, which corresponds well to the smooth nature of this inversion.

We apply now the LQL inversion with focusing to the same tri-axial instrument data. Figure 6 presents the inversion result. The gray area shows the resistive layer obtained by the LQL inversion with image focusing. The value of the anomalous conductivity is close to the true value, and the shape and location of the layer are recovered reasonably well. In particular, close to the borehole, we reconstruct exactly the true thickness of the resistive formation, while further away from the borehole the thickness of the recovered image increases, which can be explained by the decreasing sensitivity of the logging data to the structures at some distance from the borehole. Note that the dashed lines in Figures 3 and 4 indicate the fields predicted by the inverse model. One can see that the observed and predicted data fit extremely well. Therefore, the observed differences in geometry of the true model (Figure 2) and of its image (Figure 6) are caused by the limits in resolution power of the considered tri-axial induction instrument. We notice however that these differences are very small and the inverse model provides an adequate representation of the true resistive structure.

The inversion of the tri-axial induction tool data for this model required approximately 1.5 minutes of CPU time on a 1 GHz PC for smooth inversion and approximately 4 minutes for the LQL inversion with image focusing.

For comparison, we also show in Figure 7 the results of inversion of z-component data only, observed for the same model. In other words, we assume that we use the conventional induction logging instrument with only z-oriented receivers. One can see in this figure that the model generated as the result of inversion represents a ring-type structure, symmetrical with respect to the borehole axis. This result demonstrates once again that the conventional induc-

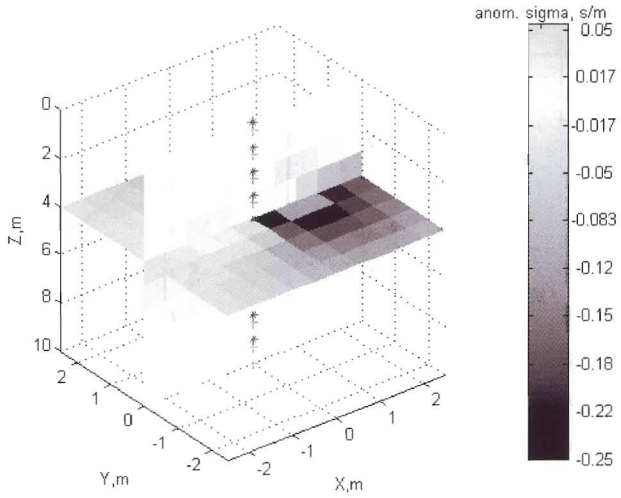

FIG. 5 The result of the smooth inversion of the tri-axial induction instrument data (with one vertical transmitter dipole) for Model 1. The gray area shows the resistive layer obtained by the LQL inversion.

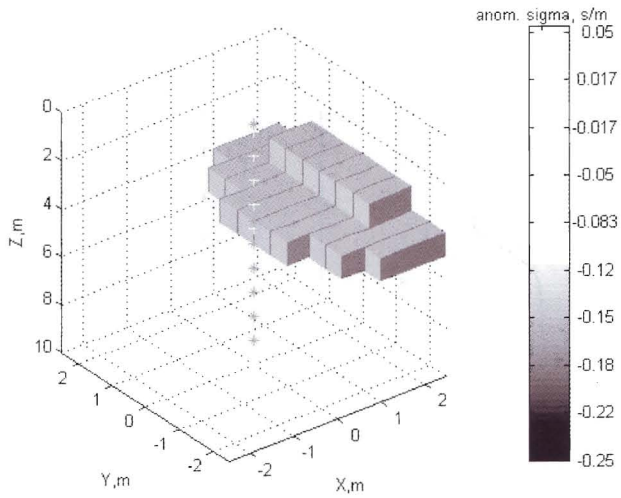

FIG. 6 The result of the tri-axial induction instrument data inversion for Model 1. The gray area shows the resistive layer obtained by the LQL inversion with image focusing.

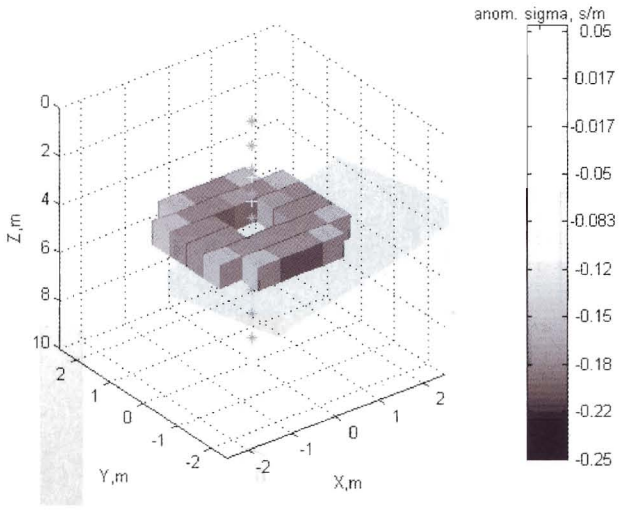

FIG. 7 The result of inversion of the data measured by the conventional induction sonde with z-oriented transmitter and receivers for Model 1. The gray area shows the resistive ring-type structure obtained by LQL inversion with image focusing.

tion logging instrument, with only z-directed transmitters and receivers, does not have directional sensitivity. The conventional logging data "see" the rock formations only as an axial-symmetric structure, which is not always the case in reservoir studies.

In the second set of numerical experiments we consider an instrument that comprises three mutually orthogonal transmitter coils located at one point and similar receiver coils located at another point (Figure 8). This instrument responds to three mutually orthogonal components of the magnetic fields excited by each of three mutually orthogonal transmitters, the responses comprising a nine-component induction tensor (Zhdanov et al., 2000a, b),

$$\hat{\mathbf{H}} = \begin{bmatrix} \mathbf{H}_x^x & \mathbf{H}_x^y & \mathbf{H}_x^z \\ \mathbf{H}_y^x & \mathbf{H}_y^y & \mathbf{H}_y^z \\ \mathbf{H}_z^x & \mathbf{H}_z^y & \mathbf{H}_z^z \end{bmatrix},$$

where superscripts refer to the transmitter components and subscripts refer to the receiver components.

Figure 9 shows Model 2 with two conductive layers located at a distance of 0.5 m from the borehole. The background conductivity is of 0.025 S/m and the anomalous conductivity is of 0.075 S/m. The instrument is moving in the vertical direction with observation points located every 1 m. The operating frequencies are 1, 10, and 100 KHz.

We use the same discretization of the region for inversion, as in the case of the single component transmitter, considered above. Figure 10 presents the result of the smooth inversion of the tensor induction instrument data. The gray areas show the conductive layers obtained by the LQL inversion. The layers obtained as the result of inversion appear to be at the right location. However, the image is unfocused and the edges of the layers are diffused, as one should expect from the smooth inversion. Figure 11 shows the result obtained by the LQL inversion with image focusing. The layers obtained as the result of inversion have the same thickness and appear to be at the same distance from

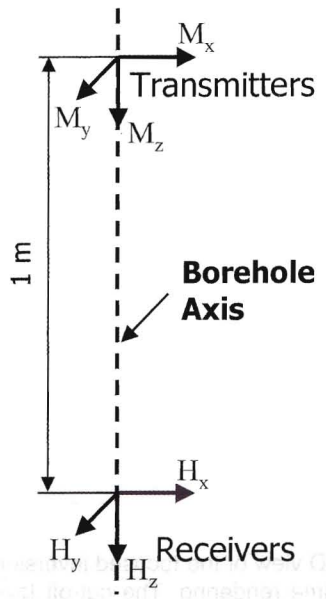

FIG. 8 Tensor induction instrument with three mutually orthogonal transmitters and a triple of mutually orthogonal receivers located at a distance of 1 m from the transmitters.

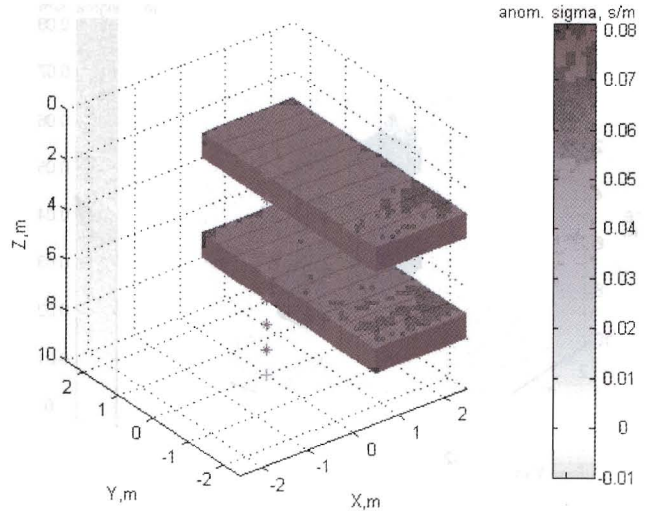

FIG. 9 Model 2 of two conductive layers located at a distance of 0.5 m from the borehole. The transmitter locations are shown by the stars.

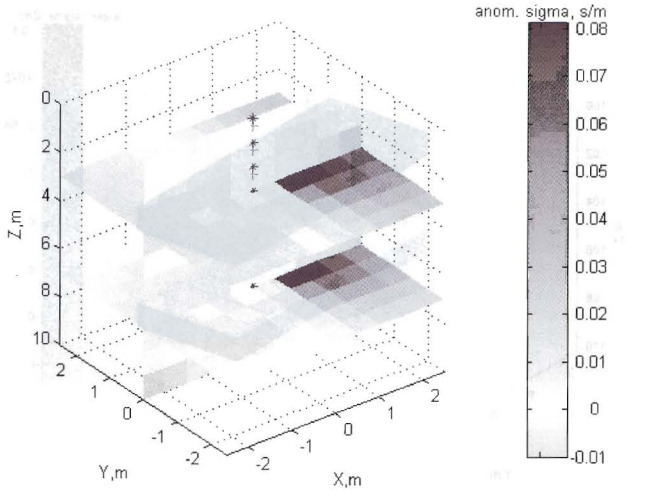

FIG. 10 The result of the smooth inversion of the tensor induction instrument data for Model 2. The gray areas show the conductive layers obtained by the LQL inversion.

the borehole as in the true model. The value of the anomalous conductivity is recovered perfectly (0.075 S/m). However, the extent of the layers is slightly smaller than in the true model (Figure 9).

Note that the LQL inversion of the tensor induction tool data for this model required approximately 3 minutes of CPU time on a 1 GHz PC for smooth inversion and approximately 10 minutes for the LQL inversion with image focusing.

Figure 12 shows Model 3 of one resistive layer with a conductivity of 0.01 S/m and one conductive layer with a conductivity of 0.1 S/m located on one side of the borehole. The background conductivity is 0.05 S/m. The anomalous conductivity is of -0.04 S/m for the resistive layer and of 0.05 S/m for the conductive layer.

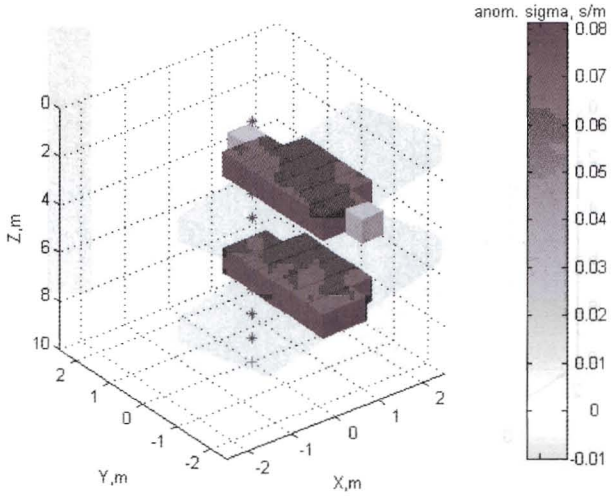

FIG. 11 The result of the tri-axial induction tool data inversion for Model 2. The gray areas show the conductive layers obtained by the LQL inversion with image focusing.

The result of the LQL inversion for this model with image focusing is shown in Figure 13. The conductive and resistive layers have the correct thickness and appear in the right positions in this image. The recovered anomalous conductivity is close to the true conductivity of both the resistive and the conductive formations. This example illustrates that the developed imaging technique does not have any specific preference in reconstructing either resistive or conductive targets, and can be applied to the study of rock formations with varying electrical properties.

Model 4 represents two resistive zones with a resistivity of 100 Ohm-m in a layered formation located on one side of the borehole. The background model is formed by a sequence of layers with the different resistivities and thicknesses as shown in Figure 14. The background resistivity of the layers containing the resistive formations is 20 Ohm-m, so that the anomalous conductivity is of -0.04 S/m. We consider this model to demonstrate that our imaging method is not restricted to a homogeneous background only. Actually, this technique can be used to image a 3D formation with an arbitrary layered background conductivity.

As in the previous models, the tensor induction instrument is moving in the vertical direction with the observation points located every 1 m. The operating frequencies are

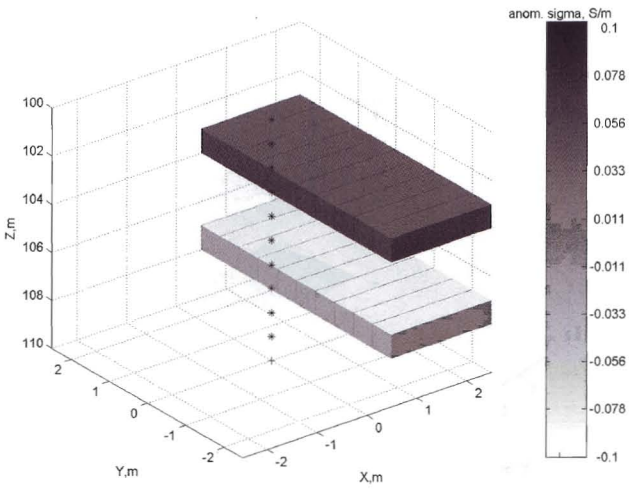

FIG. 12 Model 3 of one resistive and one conductive layer located at a distance of 0.5 m on one side of the borehole. The transmitter locations are shown by the stars.

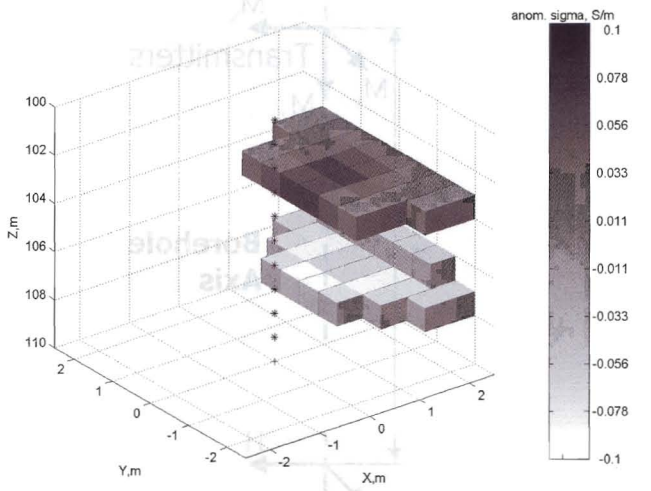

FIG. 13 A 3D view of the focused inversion result for Model 3 with the volume rendering. The cut-off level for this image is equal to 0.02 S/m for the conductive layer and to -0.016 S/m for the resistive layer. This means that only those cells with a value of anomalous conductivity greater then 0.02 S/m and less than -0.016 S/m are displayed.

the same as for Models 2 and 3. The synthetic magnetic data for this model were also computed using the integral equation forward modeling code INTEM3D and were contaminated by 2% random noise.

The result of the LQL inversion for this model with image focusing is shown in Figure 15. Note that in this case we have constrained the thickness of the resistive formations by the known thickness of the background layers hosting these formations. We present in Figure 15 a 3D distribution of the anomalous conductivity only. The anomalous conductivity, depth, horizontal extend, and thickness of the resistive zones are recovered quite well in this image. This example shows that using a priori constraints on the model parameters improves the resolution of the method.

In conclusion of this section, we should note that the models considered above may look simple and unrealistic in comparison with the real complex structure of geological formations encountered by practical well logging. However, the reader should keep in mind that this is just the first step on the difficult transition from conventional 1D interpretation models to more realistic 3D models. Our goal is to prove that the emerging new technology of tensor induction well logging could add a completely new dimension to well logging data analysis. To underscore the importance and utility of this new technique, we present in the following section a more realistic example of a practical application of the developed technology.

APPLICATION OF SINGLE-HOLE ELECTROMAGNETIC IMAGING TO RESERVOIR MONITORING

A potential application of borehole EM imaging is reservoir monitoring. Reservoir monitoring has recently emerged as a separate and important area in reservoir geophysics, as one that integrates different geophysical methods (Charara et al., 2001). Of particular interest is oil-water contact monitoring below horizontal wells, so as to adequately optimize drainage. For this purpose, for example, permanent sensors, such as electrodes (Kleef et al., 2001) or induction coils, have to be installed downhole. We will demonstrate in this section that a similar task can be performed by tensor induction well logging (TIWL) in the horizontal well.

Figure 16 shows a model typical for reservoir monitoring. The model consists of three conductive layers formed by the shale with a resistivity of 10 ohm-m, pay zone with a resistivity of 100 ohm-m, and the water-containing reservoir with a resistivity of 1 ohm-m, respectively. The waterfront has an uplifted part shown in the center of the model. We simulate a horizontally oriented (along a horizontal borehole axis) magnetic dipole transmitter, and two triples of mutually orthogonal receivers located at the distances 0.33 m and 1 m from the transmitter respectively. The operating frequencies are 1, 10, and 100 kHz. The instrument is moving in the horizontal direction with the observation points located every 1 m. We use the integral equation forward modeling code INTEM3D to simulate induction data collected along the horizontal well. We invert this synthetic data to recover the geometry of the 3D waterfront distribution.

This model is very challenging because the resistivity background is not homogeneous but layered; the induced

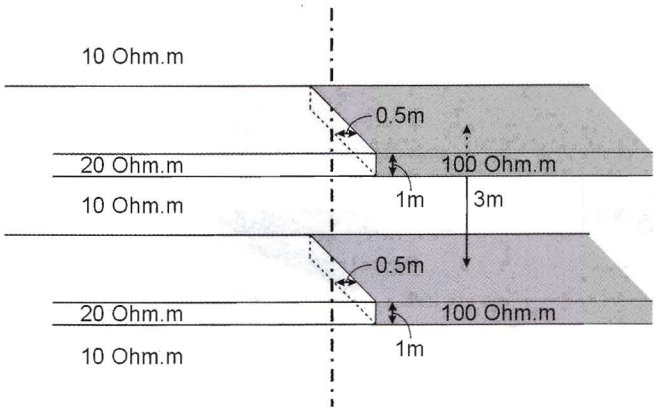

FIG. 14 Model 4 of two resistive zones in the layered formation located at a distance of 0.5 m on one side of the borehole. The background model is formed by a sequence of layers with different resistivities and thicknesses.

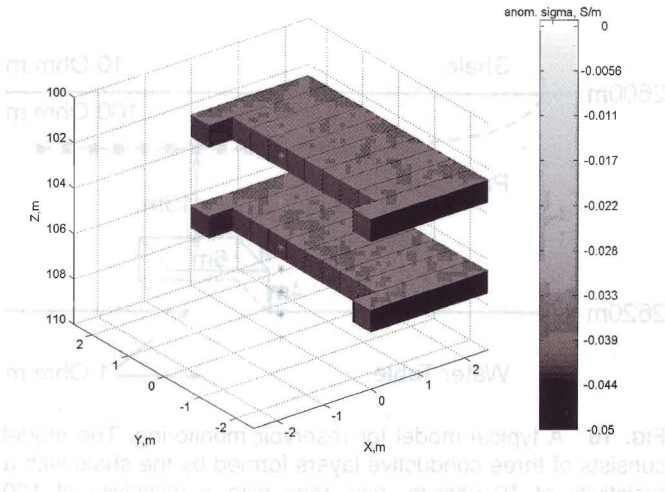

FIG. 15 A 3D view of the focused inversion result for Model 4 with the volume rendering. The cut-off level for this image is equal to -0.03 S/m for the resistive layer. This means that only those cells with a value of anomalous conductivity less than -0.03 S/m are displayed.

currents in the formation cut across layer interfaces due to the source orientation, and the 3D anomaly is located quite close to the transmitters. The area of inversion was 14 x 10 x 10m^3 and it was divided into cubic cells with 1 m sides.

Figure 17 shows a 3D image of the uplifted part of the waterfront for the true model (upper panel), and an image of the corresponding inversion result (lower panel). We can successfully locate the approaching waterfront and we approximately recover its 3D shape, although its resistivity is overestimated. This example demonstrates that 3D imaging from a single borehole provides a unique possibility to remotely detect an approaching waterfront in a petroleum reservoir. This is just one possible example of the practical application of the developed method.

DISCUSSION AND CONCLUSION

The tri-axial induction instrument was originally introduced to resolve anisotropic properties of the formation (Kriegshauser et al., 2000). However, this tool may find another important application. The tensor (tri-axial) induction instrument has a directional sensitivity which allows finding the correct location of 3D resistive or conductive targets from single-hole data. It can be used for the directional probing of the rock formations surrounding the borehole. This application may be extremely important in reservoir evaluation and monitoring of the oil/water contact. The conventional induction logging instrument (with the transmitter and receiver oriented along the borehole) usually provides an image of the resistivity distribution which is axially symmetric with respect to the borehole axis.

We have developed a rapid technique for 3D inversion of the tensor induction tool data based on the novel localized quasi-linear (LQL) approximation of the electromagnetic field. Our study demonstrates that the LQL approximation can be effectively used for 3D imaging from a single borehole. The main advantage of this technique is that the LQL approximation makes it possible to run inversion simultaneously for all transmitter and receiver positions. As a result, the LQL inversion is extremely fast and can be done in near-real time (within a few minutes), which is important for practical well logging applications. This demonstrates that the method can be used as the basis for a fast 3D imaging from a single borehole.

We have selected a set of simple models of local inhomogeneities located in the vicinity of the borehole to illustrate the developed imaging technique. Note that at this early stage of the development of the new imaging technology, we did not try to represent the real complex petrophysical models of a petroleum reservoir. Neverthe-

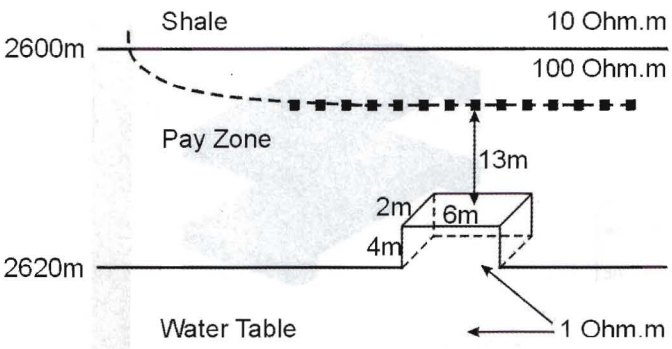

FIG. 16 A typical model for reservoir monitoring. The model consists of three conductive layers formed by the shale with a resistivity of 10 ohm-m, pay zone with a resistivity of 100 ohm-m, and the water-containing reservoir with a resistivity of 1 ohm-m, respectively. The waterfront has an uplifted part shown in the center of the model. A tri-axial induction logging instrument is run in the horizontal well passing at an elevation of 17 meters above the waterfront base.

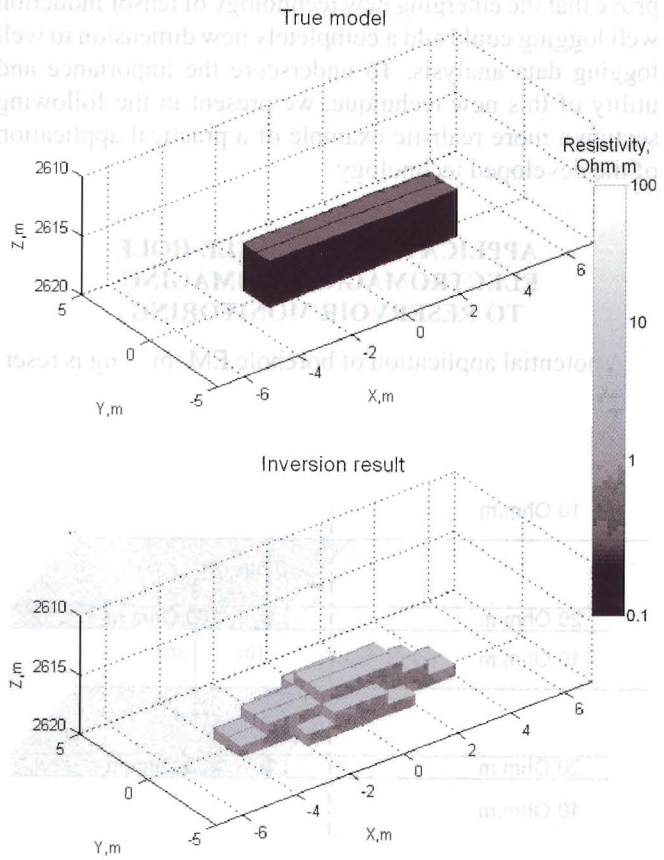

FIG. 17 A 3D image of the uplifted part of the waterfront for the true model (upper panel). An image of the inversion result obtained for the uplifted part of the waterfront (lower panel).

less, our simple model study demonstrates that the tri-axial (tensor) induction instrument can be effectively used for 3D imaging from a single borehole. Future research will be focused on a more intensive study of this emerging new technology for 3D reservoir characterization.

ACKNOWLEDGMENTS

The authors acknowledge the support of the University of Utah Consortium for Electromagnetic Modeling and Inversion (CEMI), which includes Baker Atlas Logging Services, BHP Billiton World Exploration Inc., Electromagnetic Instruments, Inc., ExxonMobil Upstream Research Company, INCO Exploration, MINDECO, Naval Research Laboratory, Rio Tinto-Kennecott, Shell International Exploration and Production Inc., Schlumberger Oilfield Services, and Sumitomo Metal Mining Co.

Special thanks are extended to M. Charara, J. P. Delhomme, and Y. Manin for their useful ideas and suggestions.

REFERENCES

Alumbaugh, D. L. and Wilt, M. J., 2001, A numerical sensitivity study of three dimensional imaging from a single borehole: *Petrophysics*, vol. 42, no. 1, p. 19–29.

Charara, M., Manin, Y., Bacquet C., and Delhomme, J. P., 2001, Combined use of permanent resistivity and transient pressure measurements for time-lapse saturation mapping, SPE –72148: Society of Petroleum Engineers, presented at Asia Pacific Oil Recovery Conference.

Cheryauka, A., Zhdanov, M. S., and Sato, M., 2001, Induction logging with directional coil polarization: modeling and resolution analysis: *Petrophysics*, vol. 42, no. 4, p. 227–236.

Doll, H. G., 1949, Introduction to induction logging and application to logging of wells drilled with oil based mud: *Journal of Petroleum Technology*, vol. 1, p. 148–162.

Habashy, T. M., Groom, R. W., and Spies, B. R., 1993, Beyond the Born and Rytov approximations: A nonlinear approach to electromagnetic scattering: *Journal of Geophysical Research*, vol. 98, no. B2, p. 1759–1775.

Hursan, G. and Zhdanov, M. S., 2002, Contraction integral equation method in 3-D electromagnetic modeling: *Radio Science*, vol. 37, no. 6, 1089, doi: 10.1029/2001RS002513, 2002.

Kleef, R. van, Halkvoort, R., Bhushan, V., El Khodhori, S. S., Boom, W. W., de Bruin, C. C. G. M., Babour, K., Chouzenoux, C., Delhome, J. P., Manin, Y., Pohl, D., Rioufol, E., Charara, M., and Harb, R., 2001, Water flood monitoring in an Oman carbonate reservoir using a downhole permanent electrode array, SPE-68078: Society of Petroleum Engineers, presented at Middle East Oil Show and Conference.

Kriegshauser, B., Fanini, O., Forgang, S., Itskovich, G., Rabinovich, M., Tabarovsky, L., Yu, L, and Epov, M., 2000, A new multicomponent induction logging tool to resolve anisotropic formation, paper D, *in* 41st Annual Logging Symposium Transactions: Society of Professional Well Log Analysts.

Kriegshauser, B., Fanini, O., Yu, L., Horst, M. and Popta, J., 2001, Improved shale sand interpretation in highly deviated and horizontal wells using multicomponent induction log data, paper S, *in* 42nd Annual Logging Symposium Transactions: Society of Professional Well Log Analysts.

Moran, J. H. and Gianzero, S., 1978, Effects of formation anisotropy on resistivity measurements: *Geophysics*, vol. 4, p. 1266–1286.

Moran, J., 1981, Apparatus and method for determining dip and/or anisotropy of formations surrounding a borehole: U.S. Patent 4,302,723.

Portniaguine, O., and Zhdanov, M. S., 1999a, Parameter estimation for 3-D geoelectromagnetic inverse problems, *in* M. Oristaglio and B. Spies, eds., *Three-dimensional electromagnetics*: Society of Exploration Geophysicists, Tulsa, p. 222–232.

Portniaguine, O. and Zhdanov, M. S., 1999b, Focusing geophysical inversion images: *Geophysics*, vol. 64, no. 3, p. 874–887.

Sato, M., Niitsuma. H., Fuziwara, J., and M. Miyairi, 1996, Apparatus and method for determining parameters of formations surrounding a borehole in a preselected direction: U.S. Patent 5,508,616.

Tartaras, E., Zhdanov, M. S., and Balch, S., 2001, Fast 3-D inversion of multi-source array electromagnetic data collected for mineral exploration, Paper PF 1.4 *in* 71st Annual International Meeting, Expanded Abstracts: Society of Exploration Geophysicists, p. 1439-1442.

Tikhonov, A. N. and Arsenin, V. Y., 1977, *Solution of ill-posed problems*: V.H. Winston and Sons, 258 pp.

Torres-Verdin, C. and Habashy, T. M., 1994, Rapid 2.5-dimensional forward modeling and inversion via a new nonlinear scattering approximation: *Radio Science*, vol. 29, no. 4, p. 1051–1079.

Zhdanov, M. S., 1988, *Integral transforms in geophysics*: Springer-Verlag, Berlin, Heidelberg, New York, London, Paris, Tokyo, 367 p.

Zhdanov, M. S., Kennedy, D., and Peksen, E., 2001a, Foundations of tensor induction well-logging: *Petrophysics*, vol. 42, no. 6, p. 588–610.

Zhdanov, M. S., Kennedy W. D., Cheryauka, B. A. and Peksen, E., 2001b, Principles of tensor induction well logging in a deviated well in an anisotropic medium, paper R, *in* 42nd Annual Logging Symposium Transactions: Society of ProfessionalWell Log Analysts.

Zhdanov, M. S. and Tartaras, E., 2002, Three-dimensional inversion of multitransmitter electromagnetic data based on the localized quasi-linear approximation: *Geophysical Journal International*, vol. 148, no. 3, p. 506–519.

Zhdanov, M. S., 2002, *Geophysical inverse theory and regularization problems*: Elsevier, Amsterdam, London, New York, Tokyo, 628 p.

ABOUT THE AUTHORS

Michael S. Zhdanov joined the University of Utah as a full professor in 1993 and he has been Director of the Consortium for Electromagnetic Modeling and Inversion since 1995. He received a PhD in 1970 from Moscow State University. He spent more than twenty years as a Professor at the Moscow Academy of Oil and Gas, as the head of the Department of Deep Electromagnetic Study and Deputy Director of IZMIRAN, and later as Director of the Geoelectromagnetic Research Institute of the United Institute of Physics of the Earth, Russian Academy of Science, Moscow, Russia, before moving to the University of Utah. In 1990 he was awarded an Honorary Diploma of Gauss Professorship by Göttingen Academy of Sciences, Germany. In 1991, he was elected Full Member of the Russian Academy of Natural Sciences. He became Honorary Professor of the China National Center of Geological Exploration Technology in 1997, and a Fellow of Electromagnetics Academy, USA, in 2002.

Efthimios Tartaras is currently a geophysicist with Schlumberger Water Services in France. He joined Schlumberger Riboud Product Centre near Paris as a Post-doctoral Researcher in 2001 to work on reservoir monitoring applications. He received his MSc and PhD degrees in geophysics from the University of Utah, where he worked on fast imaging and inversion algorithms for the interpretation of EM data.

Alexander Gribenko is a PhD student at the University of Utah. He received his MS in geosciences from Texas Tech University, Lubbock, TX in 2001, and his MS in geophysics from Novosibirsk State University, Novosibirsk, Russia in 1998. He has worked as a Research Associate at the Research Institute of Geophysics of the Siberian Branch of the Russian Academy of Sciences from 1996 to 1999 and as a Research/Teaching Assistant at Texas Tech from 1999 to 2001. His current research interests include the application of electromagnetic methods to hydrocarbon and mineral exploration.